Removal of bisphenol A over a separation free 3D Ag_3PO_4-graphene hydrogel via an adsorption-photocatalysis synergy

Chenfan Mu [a], Yu Zhang [a], Wenquan Cui [a,*], Yinghua Liang [a], Yongfa Zhu [b,*]

[a] College of Chemical Engineering, Hebei Provincial Key Laboratory of Environmental Photo & Electro Catalysis Materials, North China University of Science and Technology, Tangshan 063009, China
[b] Department of Chemistry, Tsinghua University, Beijing 100084, China

ABSTRACT

Here we reported a silver phosphate/graphene hydrogel (Ag_3PO_4/rGH) with efficient degradation of bisphenol A (BPA) with the synergy of adsorption and photocatalysis. The Ag_3PO_4/rGH 3D structure exhibits enriched adsorption-photocatalytic degradation ability for the removal of BPA under visible-light irradiation, and its three-dimensional structure facilitates the rapid recycle and reuse ability of the photocatalyst. The maximum adsorption capacity was 15 mg/g which is 2.1 times and 2.4 times than that of Ag_3PO_4/AC, Ag_3PO_4/Al_2O_3. The BPA could be even 100% removed in 12 min by the synergy of adsorption and photocatalysis under visible light irradiation. The removal ability was more than 90% after recycling 5 time indicating superiority of separation freely without complicated filter system for 3D structured hydrogel. The Ag_3PO_4/rGH 3D structure also showed high removal activity and stability in the continuous flow reaction system, and the 100% removal of BPA have been maintained more than 60 h. In all, Ag_3PO_4/rGH 3D structure possesses superiority of separation freely without complicated filter system.

© 2017 Elsevier B.V. All rights reserved.

1. Introduction

With the development of economy and industry, plentiful pollutants have been discharged into the environment, which is a serious threat to the environment and human health. Photocatalysts can effectively utilize the solar energy to degrade many toxic organic compounds in the environment and thus have attracted considerable attentions [1]. Conventional photocatalysts, such as TiO_2, have no response to visible light and their quantum yields are usually low, which limit their practical application.

Ag_3PO_4 is a new semiconductor photocatalyst that has a strong absorption and utilization ability of the visible lights with wavelengths shorter than 530 nm [2]. Its quantum yield for the oxygen evolution from water can be up to 90% under the visible light [3], and its photocatalytic degradation of organic pollutants is several times higher than that of $TiO_{2-x}N_x$ photocatalysts [4], indicating its fascinating large scale application potential. Although this, Ag_3PO_4 is suffered from its instability due to the photo-corrosion by the photo-generated electrons and thus restricted the phosphoric acid silver light absorption and degradation of pollutants. Ag_3PO_4 and

its composites also possess low specific surface areas [5], weak carrier mobility [6,7] and lower organic matter absorption abilities, limiting its photocatalytic efficiency. Scientists have combined Ag_3PO_4 with the conventional adsorbent materials, such as activated carbon [5], to increase its specific surface area and pollutant adsorption capacity for the photocatalytic degradation. The adsorption is mainly occurred on the interface of the active carbons which possesses huge internal pores and internal surface area, while the photocatalytic degradation would occurred on Ag_3PO_4 particles which gathered on the outside of active carbons. This may limit the pollutant removal ability of Ag_3PO_4.

Graphene is a nonporous absorbent with a high specific surface area and low porosity [8–11], showing a high adsorption-desorption rate and capacity in removal of organic pollutants [12–14], compared with the activated carbon and other conventional absorbents. The graphene hydrogel (rGH) with unique three-dimensional (3D) network structure in micrometer scale could be assembled from two-dimensional graphemes nano-sheets by the π-π conjugation, and own the superiority of separation freely without complicated filter system [15–17]. Reports showed that rGH has been applied in absorbing organic dyes [18], such as methyl blue (MB) [19,20], malachite green (MG) [21], rhodamine B (RHB) [22] and methyl orange (MO) [23–25]; heavy metal ions, such as Pb^{2+}, Cd^{2+} [26] and Cr (VI) [27]; gases, such as CO_2 [28] and HCHO [29]; etc., indicating that it has a great application prospect

in the adsorption and purification. Based on this, we have embedded TiO_2 nano particles in rGH system, showing enrich adsorption and photocatalytic removal of Cr(VI), in our previous reports [30], indicating the superiority of 3D structure hydrogel of graphene in the application of synergetic adsorption-photocatalysis.

In the present work, we report a silver phosphate composite photocatalyst with high specific surface area by embedded Ag_3PO_4 nano-particles in the three-dimensional network structure of rGH, Ag_3PO_4-graphene hydrogel (Ag_3PO_4/rGH), which showed the efficient synergy removal of BPA by adsorption and in situ degradation photocatalytic decomposition under visible light irradiation. The 3D structure in micrometer scale of Ag_3PO_4/rGH also facilitates the rapid recycle of photocatalyst and improves the stability.

2. Experimental

2.1. Synthesis of Ag_3PO_4/rGH composite

2.1.1. Preparation of graphite oxide (GO)

Graphite oxide (GO) was prepared by the Hummers' method [31]. Briefly, 3.0 g graphite (325 mesh) was mixed with 70 mL of H_2SO_4 (98 wt%) in a flask and stirred for 10 min in an ice bath. 1.5 g $NaNO_3$ and 9.0 g $KMnO_4$ were added into the mixture and the resultant mixture was stirred for 3 h at a temperature lower than 20 °C. The reaction temperature was increased to 35 °C and kept for 4 h. The reaction mixture was then diluted slowly with 150 mL of deionized water, reacted at 95 °C for 2 h, and titrated with 300 mL of water and 20 mL of H_2O_2 (30 wt%), which turned the reaction solution to a khaki suspension. The suspension was centrifuged and the pellet was collected, washed with 10% HCl, dialyzed against water for 7–15 days, and centrifuged again to yield a pellet of GO.

2.1.2. Preparation of rGH

rGH was synthesized by a method reported in the literature with minor modifications [31]. 60 mg GO and 0.6 g ascorbic acid were mixed, ultro-sonicated for 1.5 h, and reacted at 95 °C for 1 h to form rGH. The obtained rGH was washed with deionized water several times and dehydrated by the freeze-drying for 24 h.

2.1.3. Synthesis of Ag_3PO_4/rGH

Same amounts of rGH were respectively added to the solutions containing 0.48 g, 0.6 g, 0.9 g, 1.2 g $AgNO_3$ in deionized water, stirred for 6 h to allow a sufficient adsorption of Ag^+ on the fully impregnated rGH surface, added with a certain amount of Na_2HPO_4 solution dropwise, and freeze-dried for 24 h to produce Ag_3PO_4/rGH composites that were respectively denoted as Ag_3PO_4/rGH (4.5%), Ag_3PO_4/rGH (6%), Ag_3PO_4/rGH (9%), and Ag_3PO_4/rGH (11%).

The Ag_3PO_4 monomer was prepared by a precipitation method. Briefly, a certain amount of $AgNO_3$ was dissolved in deionized water and stirred for 30 min. A certain amount of Na_2HPO_4 solution was added to the $AgNO_3$ solution until a yellow precipitate was formed. The precipitate was dried in an oven at 80 °C for further use.

For a comparison purpose, Ag_3PO_4/AC and Ag_3PO_4/Al_2O_3 composite photocatalysts were prepared by the same procedure.

2.2. Characterization of photocatalysts

The crystal structures and phase states of Ag_3PO_4/rGH composites were determined by X-ray diffractometry (XRD) using a Rigaku D/MAX2500 PC diffractometer operated at 40 kV and 100 mA using Cu Kα radiation in a scanning range of 5–80°. The morphologies of the composites were imaged on a Hitachi s-4800 SEM microscope. The Fourier transform infrared (FTIR) spectra were recorded on a Thermo Nicolet Avatar 370 spectrometer in the range of 4000–400 cm^{-1}. Raman spectra were recorded on a microscopic confocal Raman spectrometer (Thermo Electron DXR) under the excitation at 524 nm. The Brunauer-Emmett-Teller (BET) specific surface area was measured by the nitrogen adsorption at 77 K using a Micromeritics 3020 instrument. The chemical states were determined by X-ray photoelectron spectroscopy (XPS) using an XSAM800 apparatus. UV–vis light (UV–vis) diffuse reflectance spectra were recorded on a UV–vis spectrometer (UV1901, Puxi) in the range of 200–800 nm at the resolution of 1 nm and a scan rate of 600 nm/min with solid $BaSO_4$ slices as the reference. The slit width was set to 2 nm.

2.3. Adsorption behaviors of photocatalysts

2.3.1. Static adsorption

The static adsorption was conducted in the dark in a Pyrex glass reactor (BL-GHX-TYPE, Shanghai Bilon Instruments Co., LTD.). The Ag_3PO_4/rGH composites (0.05 g) were respectively added to 100 mL 10 ppm BPA solutions and shaken at 200 r/min at 25 ± 2 °C for 8 min. A 3 mL aliquot of the suspension was taken every 1 min, filtered with a filter membrane (0.22 μm), and analyzed on a Hitachi high performance liquid chromatograph (HPLC) to monitor the BPA concentration. The measured aliquot was poured back to the reactor immediately after the HPLC analysis was finished.

2.3.2. Static photocatalytic degradation of BPA

Photocatalytic degradation was also conducted in the Pyrex glass reactor with a 250 W metal halide lamp (Philips) and an ultraviolet light filter (λ > 420 nm, transmittance >90%) placed 10 cm above. The temperature of the reactor was maintained at 25 ± 2 °C by circulating water. A 3 mL aliquot of the suspension was taken at intervals, filtered with a filter membrane (0.22 μm), and analyzed by HPLC to monitor the BPA concentration.

2.3.3. Adsorption of BPA in a continuous flow system

The composite was packed into a 4 mm (ID) glass tube photocatalytic reactor and fed with a BPA solution in the dark at a constant flow rate $v_{(BPA)}$ = 0.16 mL/min by a peristaltic pump (YZ1515, Bao Dingqi Liheng stream Co., Ltd., Bao Ding, China). The BPA concentration in the effluent was measured by the HPLC at intervals to construct the BPA adsorption breakthrough curves of Ag_3PO_4/rGH composites. The circling runs of the reaction were performed by simply recovering catalysts by filtration using a 38 μm stainless steel mesh.

2.3.4. Synergy of adsorption and photocatalysis in a continuous flow system

The continuous flow reaction was conducted in a fixed bed polyfluortetraethylene reactor with 150 mg of Ag_3PO_4/rGH photocatalyst loaded in the groove (40 mm × 20 mm × 2 mm) and an inlet and outlet on the two sides. A 500 W xenon lamp and a UV filter (λ > 420 nm, transmittance >90%) were placed above the reactor as the light source. The BPA solution was fed by the peristaltic pump at a constant flow rate. The BPA concentration in effluent was determined by HPLC to construct the BPA adsorption breakthrough curves of Ag_3PO_4/rGH composites.

3. Results and discussion

3.1. Characterization of Ag_3PO_4/rGH composites

Fig. 1 shows the XRD patterns of graphite, GO, rGH, Ag_3PO_4/rGH, Ag_3PO_4, and Ag. The natural graphite exhibited a sharp characteristic peak of (002) at 2θ = 26.4° which corresponded to a graphene layer-to-layer spacing of 3.4 Å. The peak of GO shifted to 2θ = 11.7°,
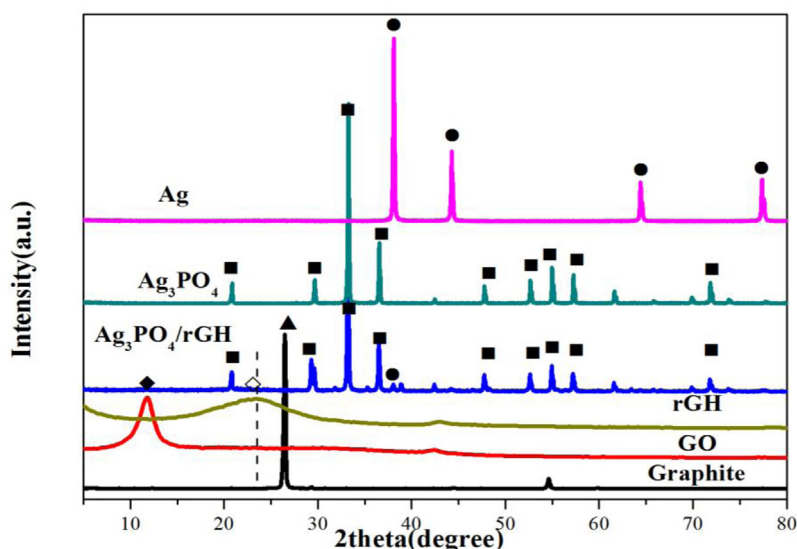
Fig. 1. XRD spectra of as-prepared graphite, GO, rGH, Ag_3PO_4/rGH, Ag_3PO_4, and Ag.

corresponding to a layer-to-layer spacing of 8.11 Å, due to the oxygen containing functional groups introduced by the oxidation. The rGH showed a new broad peak at $2\theta = 24.5°$ that corresponded to a layer-to-layer spacing of 3.67 Å and the characteristic peak of GO disappeared, indicating that GO was reduced to some extent and most of the oxygen containing functional groups were removed. In addition, the broad diffraction peak indicated that the stacking of the graphene nano-sheets of rGH was disordered. Ag_3PO_4/rGH 3D showed similar diffraction patterns to that of the body-centered cubic Ag_3PO_4 (JCPDS NO.06-0505), consistent with the previous reports [32,33]. The Ag_3PO_4/rGH showed a weak diffraction peak at $2\theta = 37.7°$ which was consistent with the characteristic peak of the (111) panel of Ag, indicating that a small amount of Ag^+ was reduced to Ag by the VC residue in rGH. No diffraction peaks of rGH were observed in the Ag_3PO_4/rGH composites. This can be explained that Ag_3PO_4 completely filled the space between the graphene layers of rGH, isolated the layers, and thus increased the degree of layer stacking disorder. In addition, the reduced rGH content in the composites also contributed to the disappearance of its characteristic peaks.

The morphologies of rGH, Ag_3PO_4, and Ag_3PO_4/rGH are shown in Fig. 2. rGH inherited the large accessible surface area of graphene, but exhibited a highly porous three-dimensional structure with pore sizes of several micrometers (Fig. 2a). The formation of this special morphology by the reduction of graphene largely relies on the hydrophobicity, intramolecular forces, and π-π conjugation [30]. The Ag_3PO_4 monomer and its body-centered cubic structure were particles with sizes up to 10 μm (Fig. 2b). As shown in Fig. 2c for the SEM image of Ag_3PO_4/rGH, the aggregation of Ag_3PO_4 were significantly reduced and large amounts of Ag_3PO_4 nanoparticles were well-distributed between the graphene layers, which inhibited the graphene layer stacking. The particle size of the Ag_3PO_4 in Ag_3PO_4/rGH composite was ~300 nm and smaller than the particle size of Ag_3PO_4 monomer (Fig. 2b). It can be explained that Ag_3PO_4 nanoparticles was wrapped by the graphene layers, which inhibited the aggregation, and thus reduced the size of Ag_3PO_4 particles. Zhu [34–36] also considered that GO could affect the morphology and particle size of photocatalyst, such as Ag/AgX. It is worth pointing out that the rich spatial reticulated structure of rGH that provides the high specific surface area of the catalyst is essential for the synergy of the surface adsorption and photocatalysis of the composite catalyst.

The formation mechanism of Ag_3PO_4/rGH by the impregnation method can be briefly described as the following, as shown in Scheme 1. GO was reduced by ascorbic acid (VC) at 95 °C to produce rGH. The excessive unreacted VC was removed by washing the gel with deionized water. The rGH was immersed in a certain concentration of $AgNO_3$ aqueous solution to allow the penetration of Ag^+ into its 3D network structure. The Ag^+ and negatively charged oxygen containing functional groups which had not been completely restore in the graphene layers by the electrostatic interaction. Na_2HPO_4 was added as a precipitating agent to produce the Ag^+/rGH suspension and eventually form Ag_3PO_4/rGH in-situ.

The high-resolution Ag *3d* XPS spectra of Ag_3PO_4/rGH composites exhibited two strong peaks at 367.5 and 373.4 eV of Ag $3d_{3/2}$ and Ag $3d_{5/2}$, respectively, indicating that most of the Ag in the composite was Ag^{+1} (Fig. 3a). Two weak peaks at 368.13 and 374.2 eV indicated the existence of small amounts of zero valent Ag that was formed by the reduction of Ag^+ by the VC [36], consisting with the XRD results. The characteristic peaks at 284.9 eV (C—C/C=C), 286.6 eV (C—O), 287.7 eV (C=O), and 287.7 eV (O=C—OH) in the C*1s* XPS chemical map of GO suggested that GO contained large amounts of oxygen containing functional groups [37] (Fig. 3b). The weak peak at 286.6 eV (C—O) in the C*1s* spectrum of self-assembly rGH (Fig. 3c) indicated that there was still certain amounts of C=O and O=C—OH residues in rGH. These hydrophilic groups are favorable to the photocatalytic activity of the composites. The C*1s* maps of Ag_3PO_4/rGH composites are similar to that of rGH and no addition peak was observed (Fig. 3d), indicating that the carbon atoms were restricted in rGH and rGH did not break the lattice of Ag_3PO_4. The UV–vis absorption analysis suggested that the introduction of rGH did not significantly change the forbidden band width of Ag_3PO_4 (Fig. S3). Therefore, Ag_3PO_4 and rGH co-existed independently in the composite and the Ag_3PO_4 lattice was not affected by the introduction of rGH [38–40]. Based on these results, the interaction between Ag_3PO_4 and rGH in the composite was further investigated by infrared and Raman spectroscopic analysis.

Fig. 4a shows the FTIR spectra of Ag_3PO_4, Ag_3PO_4/rGH, and rGH. The absorption peaks at 1051 cm^{-1} and 1391 cm^{-1} rGH were attributed to the C—O—C stretching vibration of the epoxy and alkoxy groups, and the C—OH stretching vibration, respectively. The peak at 1650 cm^{-1} was ascribed to the C=C stretching vibration of the conjugated double bond. The strong absorption peak at 3420 cm^{-1} was due the —OH stretching vibration in H_2O. The

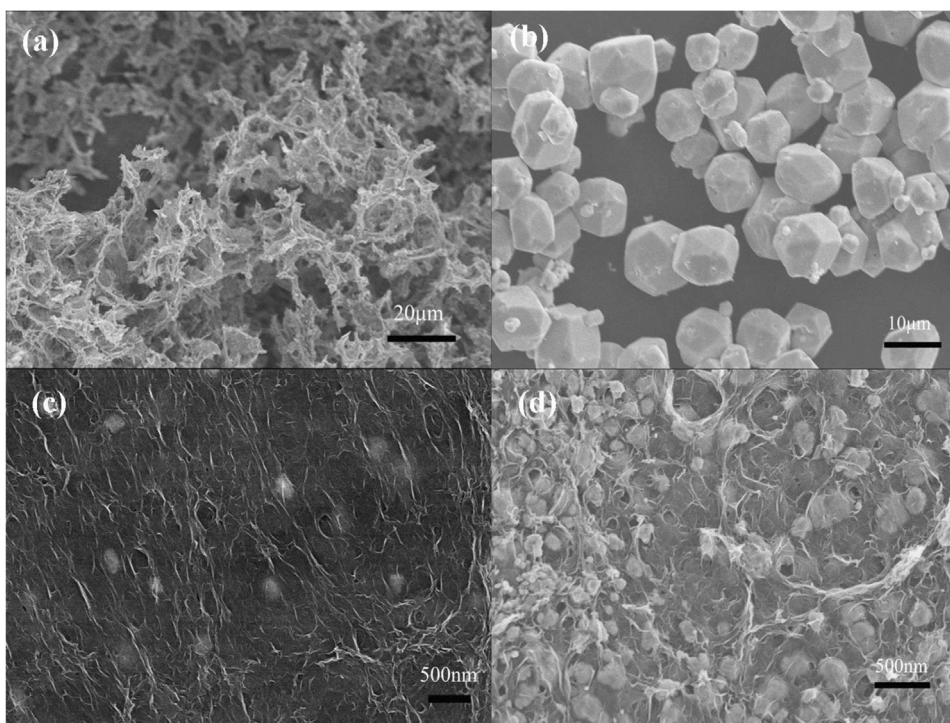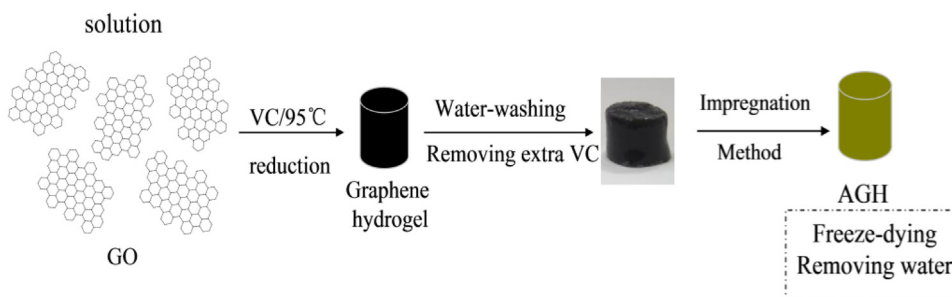**Fig. 2.** SEM images of rGH (a), Ag₃PO₄ (b), and Ag₃PO₄/rGH (c and d).

Scheme 1. Schematic of the preparation process of Ag3PO4/rGH.

absorption peaks of Ag_3PO_4 at $3420\,cm^{-1}$ and $1640\,cm^{-1}$ were assigned to the stretching vibration of —OH in the absorbed H_2O. The characteristic peak at $550\,cm^{-1}$ was due to the bending vibration of O＝P-O. The absorption peaks at $850\,cm^{-1}$ and $1097\,cm^{-1}$ were assigned to the symmetric and asymmetric stretching vibrations of P—O—P. The absorption peak at $1383\,cm^{-1}$ was ascribed to the stretching vibration of P＝O. After Ag_3PO_4 was loaded into rGH network, two new peaks appeared at $1570\,cm^{-1}$ and $1240\,cm^{-1}$ due to the skeletal vibration of graphene layers and the C—O stretching vibration in the epoxy group, respectively. These results indicated that the composite contained Ag_3PO_4 and rGH, consistent with the results of XPS analysis. The absorption peak of Ag_3PO_4 at $1097\,cm^{-1}$ that was assigned to the P—O—P stretching vibration shifted to $1122\,cm^{-1}$ in Ag_3PO_4/rGH composites, suggesting that there might be an interaction between Ag_3PO_4 and rGH in the composite. The interaction between rGH and Ag_3PO_4 is favorable to the photocatalytic activity of their composites [40].

The Raman spectra of GO, rGH, Ag_3PO_4, and Ag_3PO_4/rGH composite are shown in Fig. 4b. The distinct Raman peaks of Ag_3PO_4 at 410, 575, and $720\,cm^{-1}$ were attributed to the symmetric stretch of P—O—P and its strong absorption peak at $903\,cm^{-1}$ was ascribed to the motion of terminal oxygen in its phosphate group [41].

The Raman D and G modes of carbon materials are very sensitive to the property changes, such as defects, the degree of disorder, particle size and so on. The intensity of D peak is mainly related to the edge defects of graphene planes and the degree of disorder. The intensity of G peak is corresponding to the in-plane sp² hybridized carbon atoms of graphene. Therefore, the intensity ratio of D peak to G peak (I_D/I_G) is usually used to characterize the degree of disorder and reduction of graphene. As shown in Fig. 4b, The G peak and D peak of both GO and rGH appeared at $1600\,cm^{-1}$ and $1355\,cm^{-1}$. The I_D/I_G of rGH is higher than that of GO, suggesting that the oxygen containing groups were reduced, consistent with the previously reported [32]. Ag_3PO_4/rGH exhibited the Raman vibration peaks of Ag_3PO_4 and the D and G peaks of rGH. The I_D/I_G of the rGH in the composite was also greater than that of GO. It is worth noting that the G peak of rGH in the composite shifted from $1600\,cm^{-1}$ to $1610\,cm^{-1}$. This might be explained that the interaction between Ag_3PO_4 and the graphene layer of rGH weakened the conjugated large π bond and increased the degree of the disorder of the carbon atoms in rGH [38]. The red shift of the G peak suggested that valent bonds might be formed between rGH and Ag_3PO_4, consistent with the results of FT-IR analysis.
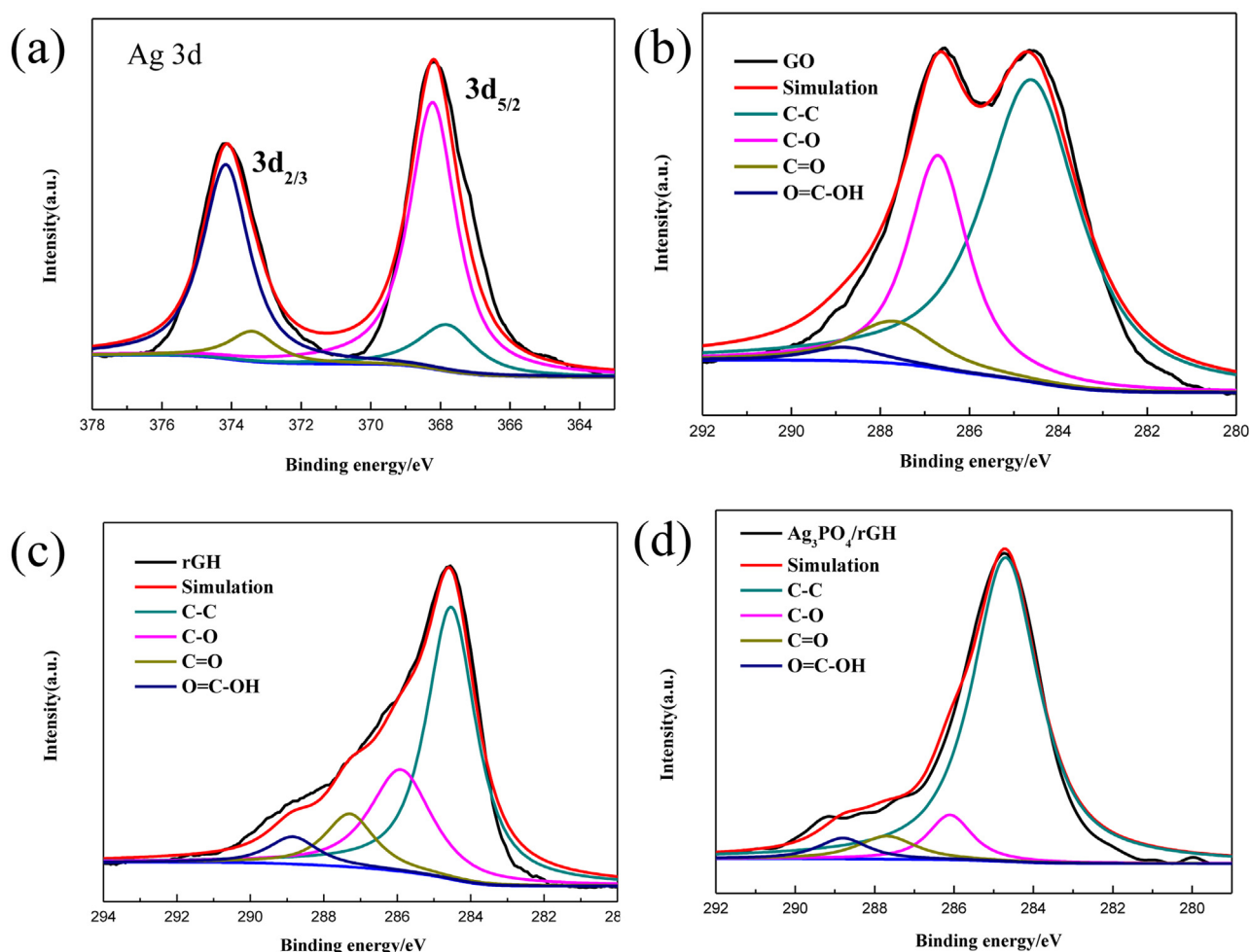
Fig. 3. High-resolution Ag $3d$ spectra of Ag_3PO_4/rGH composites (a) and the high-resolution C $1s$ spectra of the GO (b), rGH (c), and Ag_3PO_4/rGH (d).
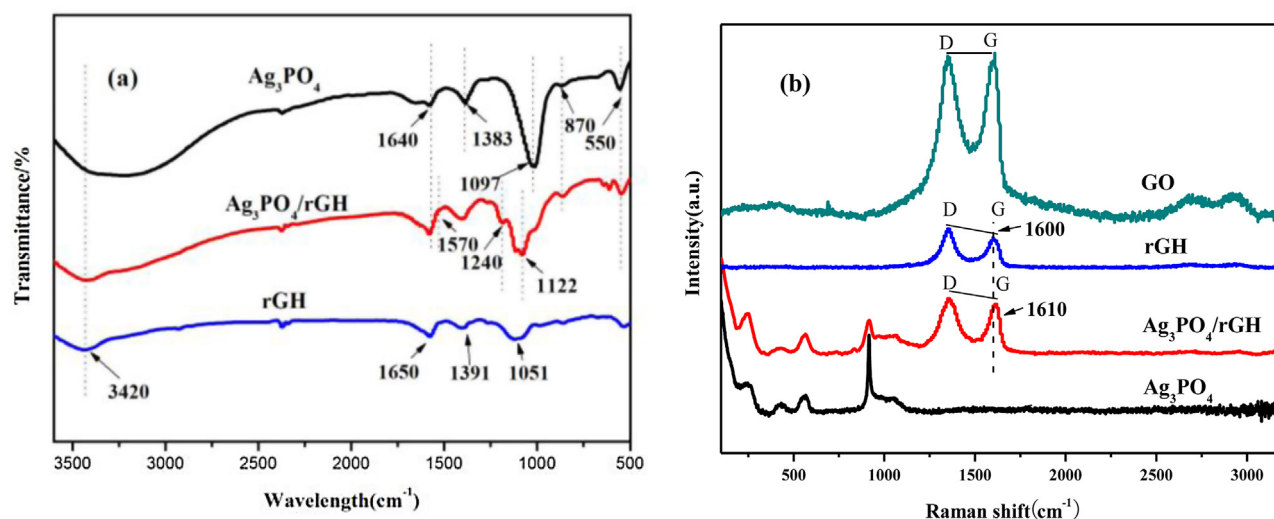
Fig. 4. FT-IR spectra of Ag_3PO_4, Ag_3PO_4/rGH, and rGH (a), and Raman spectra of GO, rGH, Ag_3PO_4, and Ag_3PO_4/rGH (b).

3.2. BPA removal by the synergy of adsorption and photocatalysis of Ag_3PO_4/rGH

3.2.1. Adsorption of BPA

Same amounts (0.05 g) of Ag_3PO_4/rGH, Ag_3PO_4/AC and Ag_3PO_4/Al$_2$O$_3$ that containing 11% rGH, AC and Al$_2$O$_3$ monomer,

respectively, and Ag_3PO_4 monomer were respectively added to 100 mL 10 ppm BPA solutions. AC and Al$_2$O$_3$ showed no significant effects on the BPA adsorption capacity of their composites with Ag_3PO_4 due to their low BPA adsorption capacity (Fig. 5a) [42,43]. In contrast, Ag_3PO_4/rGH was able to increase the BPA adsorption
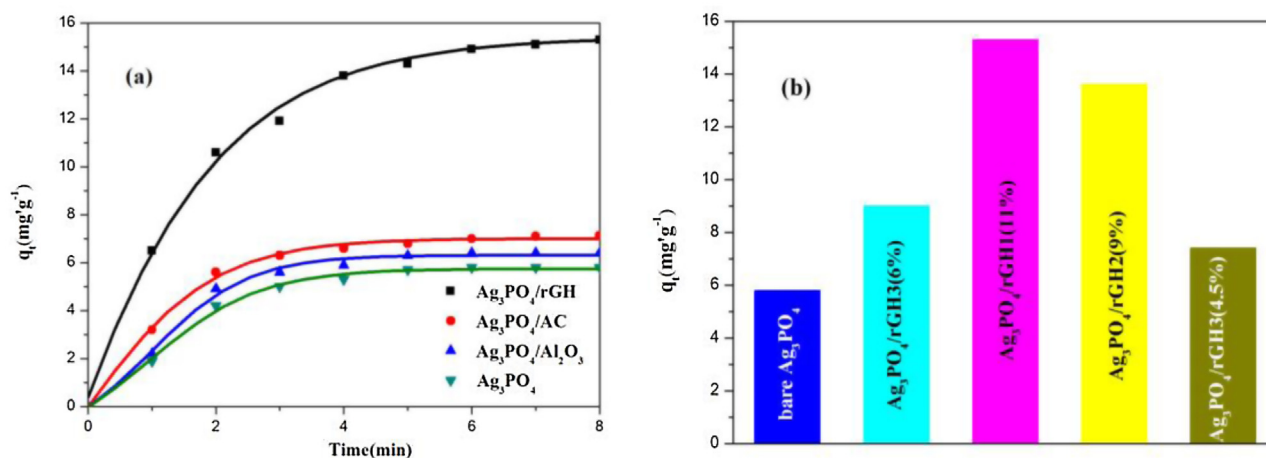
Fig. 5. (a) BPA adsorption on Ag_3PO_4/rGH, Ag_3PO_4/AC, Ag_3PO_4/Al_2O_3 and Ag_3PO_4; (b) The maximum BPA adsorption capacities of Ag_3PO_4 and Ag_3PO_4/rGH (4.5%), Ag_3PO_4/rGH (6%), Ag_3PO_4/rGH (9%), and Ag_3PO_4/rGH (11%) composites containing 4.5%, 6.0%, 9% and 11% rGH.

capacity of Ag_3PO_4 2.6 times with an equilibrium BPA adsorption capacity of 15 mg/g (Fig. 5a and Table S1). The N_2 adsorption-desorption isotherm of Ag_3PO_4/rGH was similar to that of rGH and both were S-type (Fig. S1), suggesting that Ag_3PO_4/rGH inherited the pore structure of rGH. The pore size of Ag_3PO_4/rGH ranged from 2 nm to 20 nm and it was mainly composed of mesoporous structures (Fig. S2). The specific surface area of Ag_3PO_4/rGH was 325.3 m^2/g more than that of rGH (180 m^2/g).However, the specific surface and pore volume of Ag_3PO_4/rGH were remarkably higher than those of Ag_3PO_4 monomer, Ag_3PO_4/AC, and Ag_3PO_4/Al_2O_3 (Fig. S1 and Table S1), which contributed to its high BPA adsorption capacity. The hydrophobicity of rGH could suppress the competitive adsorption of H_2O, which also increased the BPA adsorption capacity of Ag_3PO_4/rGH. In addition, Ag_3PO_4/rGH showed a higher adsorption rate than Ag_3PO_4/AC and Ag_3PO_4/Al_2O_3. The BPA adsorption of Ag_3PO_4/rGH reached 12 mg/g in 2 min and those of Ag_3PO_4/AC and Ag_3PO_4/Al_2O_3 were only 5.1 mg/g and 4.9 mg/g. In all, rGH was able to increase the specific surface area and pore volume of Ag_3PO_4, and thus greatly improved its BPA adsorption capacity and efficiency.

The rGH content in the composite can also affect the BPA adsorption capacity (Fig. 5b). The BPA adsorption capacity of Ag_3PO_4/rGH increased with the increase of rGH content. For example, the maximum BPA adsorption capacity of Ag_3PO_4/rGH (11%) composite containing 11% rGH was 15 mg/g and that of Ag_3PO_4/rGH (4.5%) composite containing 4.5% rGH was 8.4 mg/g. However, the maximum adsorption capacity of Ag_3PO_4/rGH (4.5%) was still higher than that of Ag_3PO_4/AC containing 11% AC (7.0 mg/g, Table S1). Therefore, even small amounts of rGH could significantly improve the BPA adsorption capacity of Ag_3PO_4/rGH.

3.2.2. Static BPA removal by the synergy of adsorption and photocatalysis

Fig. 6a shows the BPA removal efficiencies of Ag_3PO_4/rGH (9%), Ag_3PO_4 (equivalent), and rGH (equivalent) under same conditions. Ag_3PO_4/rGH showed a higher BPA adsorption efficiency in the dark than Ag_3PO_4, where adsorption dominated the BPA removal and BPA was pre-concentrated in the dark reaction process. The BPA adsorption on both Ag_3PO_4/rGH and rGH gradually became saturated in 30 min. The adsorbed BPA on Ag_3PO_4/rGH and Ag_3PO_4 was rapidly degraded as the light source (visible light) was turned on. Ag_3PO_4/rGH showed a little bit lower photocatalytic degradation rate than that of Ag_3PO_4 may due to the shading effect of graphene. In addition, the rGH content in the composite also affected the photocatalysis efficiency of the composite (Fig. S4). The photocatalysis

dominated the BPA removals by the composites containing low rGH contents and the photocatalytic efficiency of the composites containing high rGH contents were low, indicating the rGH inhibited the photocatalytic efficiency of the composite by the shading the catalyst from the light source.

The BPA removal efficiencies of Ag_3PO_4/AC, Ag_3PO_4/Al_2O_3, and Ag_3PO_4/rGH 3D structrue containing same Ag_3PO_4 content are shown in Fig. 6b. It is clear that the BPA removal efficiency of Ag_3PO_4/rGH is much higher than those of Ag_3PO_4/AC, Ag_3PO_4/Al_2O_3 due to the synergy of its surface adsorption and photocatalysis. The synergy of adsorption and degradation simultaneously by Ag_3PO_4 nano-particles being embedded in the three-dimensional gel structure of graphene, on which the high BPA adsorption capacity of rGH and the in-situ photocatalysis of Ag_3PO_4 were emerged and thus enriched the high BPA removal efficiency.

The synergy of adsorption and photocatalysis over Ag_3PO_4/rGH 3D structure was also significantly affected by the relative contents of rGH and Ag_3PO_4 in the composite (Fig. S5). The degree of synergy increased with the increase of rGH content firstly, and decreased thereafter, which might be due to the compatibility between the adsorption and photo-catalysis. The synergistic effect was more significant on the low concentrations of BPA, and 5 ppm BPA was almost completely removed in 12 min over the optimized ratio of Ag_3PO_4/rGH.
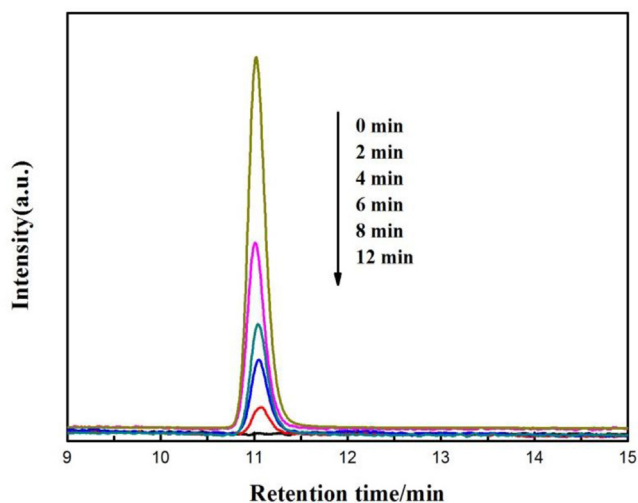
Fig. 7 shows the HPLC chromatograms of a 5 ppm BPA solution treated with Ag_3PO_4/rGH (11 wt%) for different periods of time under visible light irradiation. The BPA concentration gradually decreased with the increase of irradiation time and became undetectable in 12 min, indicating that Ag_3PO_4/rGH (11 wt%) could rapidly completely mineralization BPA due to the adsorption-photocatalysis synergistic effect. The BPA peak in the chromatograms slightly shifted with the increase of degradation due to the formation of some intermediates [44].

Fig. 8 (a) shows cycle runs of BPA degradation on Ag_3PO_4/rGH. The BPA adsorption capacity of Ag_3PO_4/rGH (9 wt%) significantly decreased after 5 cycles. However, the BPA removal efficiency after the 5 runs was still over 85% due to the adsorption-photocatalysis synergistic effect. The synergy between adsorption and photocatalysis has higher removal efficiency than pre-adsorption. The 3D structure hydrogel was freely separated on a filter and regenerated without using complex filtering system due to its 3-D network gel structure in micrometer scale. As shown in Fig. 8(b), there was formation of small Ag particles on the interface of Ag_3PO_4/rGH (9 wt%) after 5 cycles. This phase could be characterized by the appearance
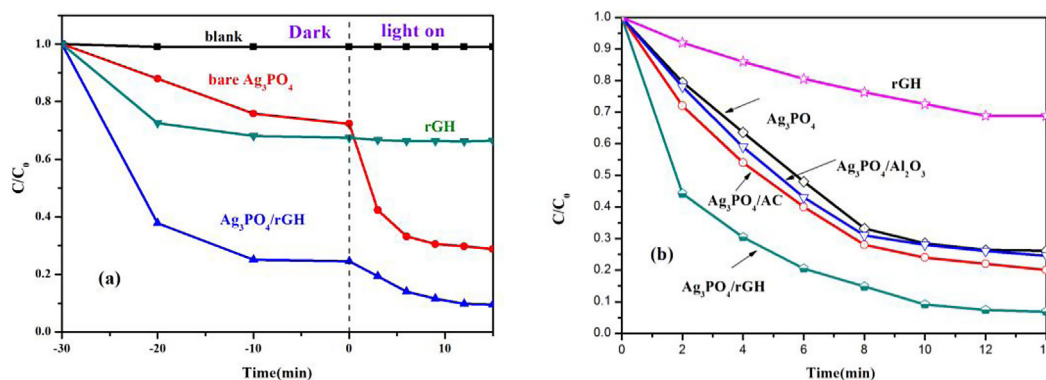
Fig. 6. (a) Comparison of photocatalytic activities of Ag_3PO_4, Ag_3PO_4/rGH and rGH for the BPA degradation; (b) Influence of different composite materials on the adsorption-photocatalysis synergistic effect.

Fig. 7. HPLC chromatograms of a 5 ppm BPA solution treated with Ag_3PO_4/rGH (11 wt%) for different periods of time.

of Bragg diffraction peaks at $2\theta = 37.7°$, $64.4°$ and $77.4°$, which were indexed to (111), (220) and (311) planes for Ag. Therefore, the incorporation of rGH into Ag_3PO_4 not only heavily enhanced the visible light photocatalytic performance of Ag_3PO_4 but also inhibited the photo-corrosion, thereby resulting in enhanced stability of Ag_3PO_4 activity. The recovery for Ag_3PO_4/rGH 3D structure was performed via a simple filtration using a 38 μm stainless steel mesh, as shown in Fig. 8c and d. No Ag_3PO_4 nano-particles could be recovered via filtration by using 38 μm stainless steel mesh, while 96% of the Ag_3PO_4/rGH 3D structure has been recovered at the same condition. Recovery percent remains above 91% even after five cycles of filtration for Ag_3PO_4/rGH 3D structure. These results indicate that the 3D structure hydrogel can be freely separated via a simple filtration and regenerated without complex separation system using high pressure and centrifuge due to its 3D network gel structure in micrometer scale.

3.2.3. BPA removal by the synergy of adsorption and photocatalysis in a continuous flow system

The BPA removal efficiency of Ag_3PO_4/rGH in a continuous flow system was investigated with 0.15 g Ag_3PO_4/rGH and a flow of 10 ppm BPA solution delivered at 0.16 mL/min. As shown in Fig. 9 for the BPA adsorption breakthrough curve of Ag_3PO_4/rGH, the complete BPA removal was lasted for 10 h and the adsorption reached the breakthrough point. However, the adsorption efficiency remained high thereafter in the certain period of time and

gradually decreased. The adsorption was saturated at 100 h. The breakthrough point and the time when the adsorption was saturated were postponed with the increase of rGH content in the composite (Fig. S7).

Fig. 10 shows the breakthrough curves of adsorption and adsorption-photocatalysis of Ag_3PO_4/rGH for the continuous BPA flow. The pre-adsorption reached the breakthrough point in 10 h. However, the BPA removal efficiency of the adsorption-photocatalysis was kept at 100% for over 60 h. It can be explained that the BPA adsorbed on the catalyst and rapidly degraded by the photocatalysis under the light irradiation, which significantly postponed the adsorption breakthrough point.

To determine the stability of the system, the transient response of Ag_3PO_4/rGH was investigated. Ag_3PO_4/rGH were saturated with BPA and exposed to the light source. No further adsorption occurred during this stage. As shown in Fig. 11 curve b, the BPA was rapidly degraded as the light turned on and the removal efficiency remained sturdy. The removal efficiency became zero as the light turned off and increased back as the light turned on again. These observations suggested that the Ag_3PO_4/rGH composite was stable and responded to the visible light rapidly. The adsorption-photocatalysis were also conducted by exposing the reactor to the light without pre-adsorption. As shown in Fig. 11 curve a, the composite exhibited almost 100% BPA removal efficiency with the light on in 30 h. As the light was turned off, the BPA removal efficiency decreased but was still maintained at a certain level due to the adsorption process. The BPA removal efficiency increased back to the original level as the light was turned on. After 50 h, the removal rate of bisphenol A decreased, but still remained above 95% .These observations indicated that the photocatalysis of Ag_3PO_4/rGH composite is instantaneous due to the synergy between its adsorption and photocatalysis.

4. Conclusion

As a summary, Ag_3PO_4/rGH 3D gel structure with synergy of adsorption and photocatalytic degradation for efficient removal of BPA was reported. Ag_3PO_4/rGH 3D structure showed the high adsorption ability and photocatalytic degradation for the removal of BPA. The graphene nano-sheet in Ag_3PO_4/rGH 3D structure showed the characteristics of non-porous surface adsorption and which can efficient adsorb the BPA. Meanwhile, the Ag_3PO_4 nano-particles anchored on graphene nano-sheet can further in situ degrade the adsorbed BPA under visible light irradiation. The maximum adsorption capacity was 15 mg/g which is 2.1 times and 2.4 times than that of Ag_3PO_4/AC, Ag_3PO_4/Al_2O_3. The BPA could be even 100% removed in 12 min by the synergy of adsorption and photocatalysis under visible light irradiation. The removal ability
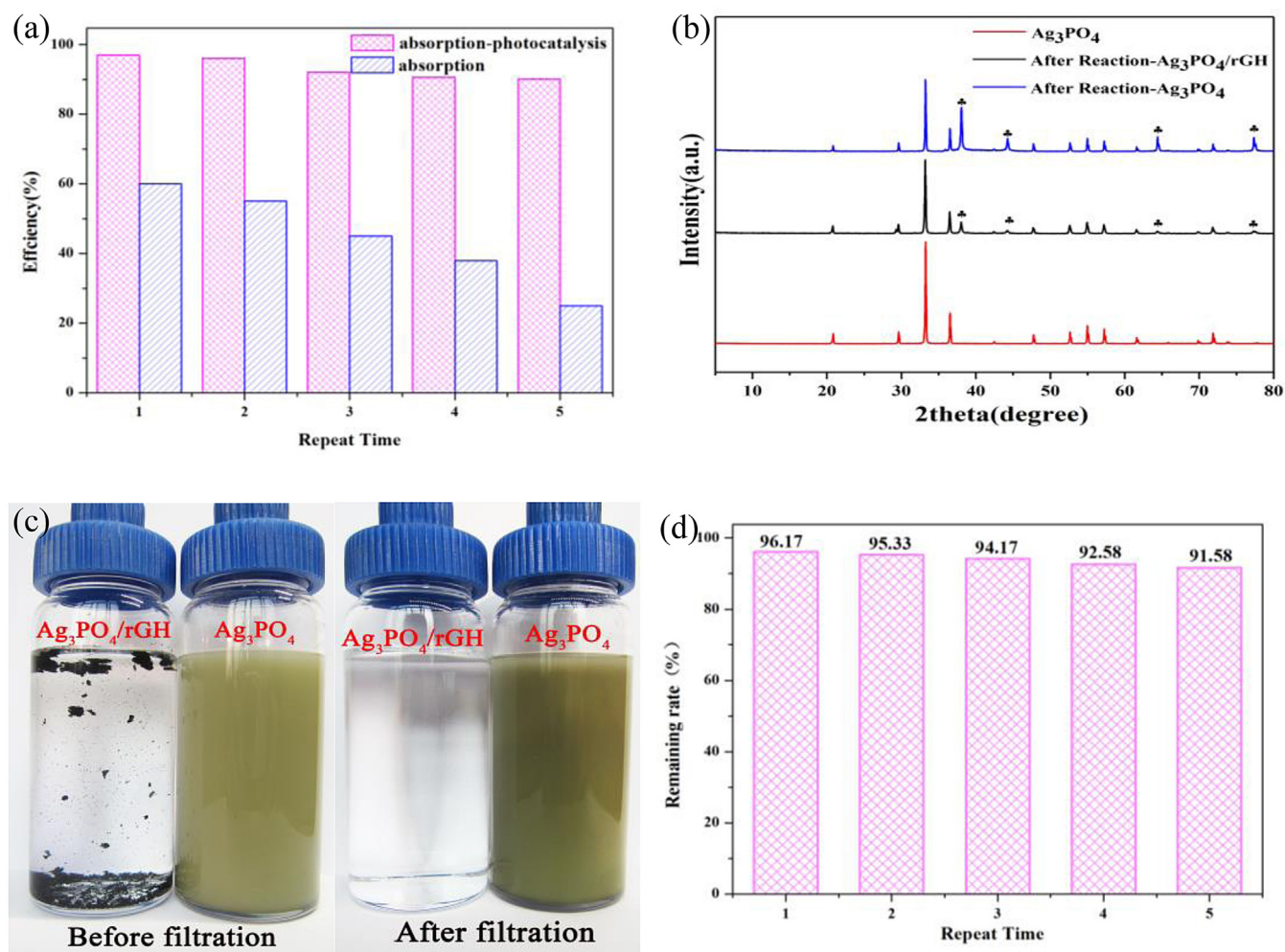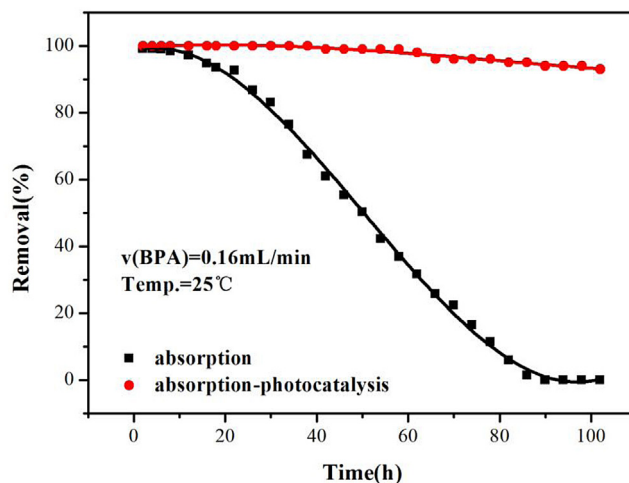
Fig. 8. (a) Cycle runs of the BPA removal by the synergistic effects of absorption-photocatalysis of Ag_3PO_4/rGH; (b) XRD spectra of before and after the photocatalytic reaction. (c) Comparison of Ag_3PO_4 and Ag_3PO_4/rGH before and after filtration; (d) Remaining rate of the Ag_3PO_4/rGH by cycle runs after filtration.
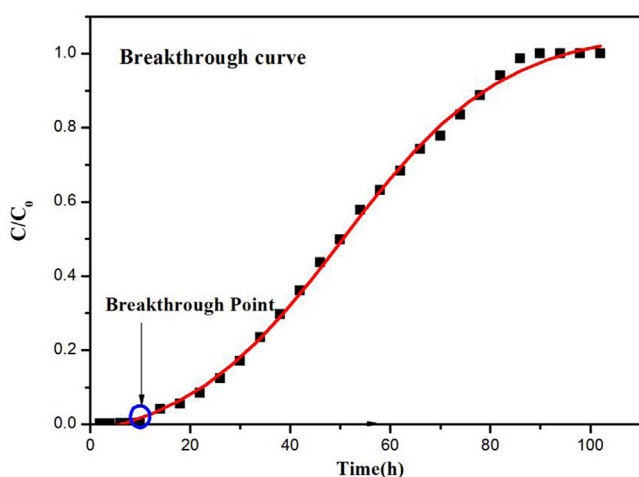
Fig. 9. Breakthrough curves for BPA absorption with Ag_3PO_4/rGH.

Fig. 10. Breakthrough curves of adsorption and adsorption-photocatalysis of Ag_3PO_4/rGH.

was more than 90% after recycling 5 time indicating superiority of separation freely without complicated filter system for 3D structured hydrogel. The Ag_3PO_4/rGH 3D structure also showed high removal activity and stability in the continuous flow reaction system, and the 100% removal of BPA have been maintained more than 60 h. In all, the Ag_3PO_4/rGH 3D structure exhibited excellent removal of organic pollutant over the synergy of adsorption and in situ photocatalysis behaviors and separation for free.
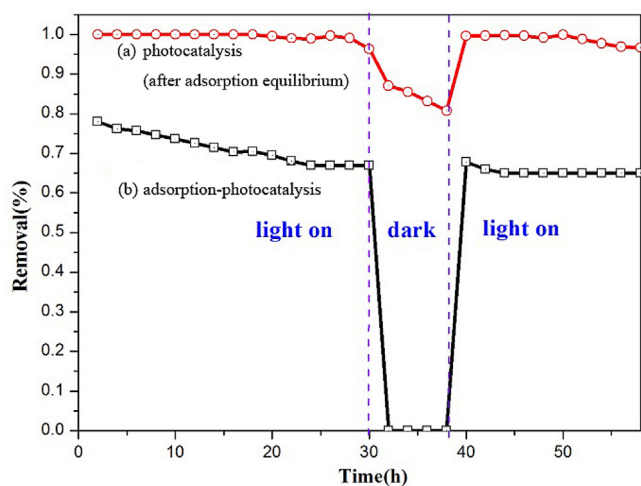
Fig. 11. Performance of Ag$_3$PO$_4$/rGH at alternating dark-light cycles under the effects of photocatalysis and absorption-photocatalysis synergistic effect separately.

Acknowledgements

Appendix A. Supplementary data

Supplementary data associated with this article can be found, in the online version, at http://dx.doi.org/10.1016/j.apcatb.2017.04.018.

References

[1] M. Ge, C. Cao, J. Huang, S. Li, Z. Chen, K.-Q. Zhang, S.S. Al-Deyab, Y. Lai, J. Mater. Chem. A 4 (2016) 6772–6801.
[2] L. Liu, L. Ding, Y. Liu, W. An, S. Lin, Y. Liang, W. Cui, Appl. Catal. B: Environ. 201 (2017) 92–104.
[3] Z. Yi, J. Ye, N. Kikugawa, T. Kako, S. Ouyang, H. Stuart-Williams, H. Yang, J. Cao, W. Luo, Z. Li, Y. Liu, R.L. Withers, Nat. Mater. 9 (2010) 559–564.
[4] M.E. Taheri, A. Petala, Z. Frontistis, D. Mantzavinos, D.I. Kondarides, Catal. Today 280 (2017) 99–107.
[5] H. Wang, Z. Ye, C. Liu, J. Li, M. Zhou, Q. Guan, P. Lv, P. Huo, Y. Yan, Appl. Surf. Sci. 353 (2015) 391–399.
[6] Y. Li, L. Yu, N. Li, W. Yan, X. Li, J. Colloid Interface Sci. 450 (2015) 246–253.
[7] L. Zhang, H. Zhang, H. Huang, Y. Liu, Z. Kang, New J. Chem. 36 (2012) 1541.
[8] H. Wang, X. Yuan, Y. Wu, H. Huang, X. Peng, G. Zeng, H. Zhong, J. Liang, M. Ren, Adv. Colloid Interface Sci. 195–196 (2013) 19–40.
[9] Y. Shen, Q. Fang, B. Chen, Environ. Sci. Technol. 49 (2015) 67–84.
[10] H. Wang, X. Yuan, G. Zeng, Y. Wu, Y. Liu, Q. Jiang, S. Gu, Adv. Colloid Interface Sci. 221 (2015) 41–59.
[11] K. Fu, J. Huang, N. Yao, X. Xu, M. Wei, Ind. Eng. Chem. Res. 55 (2016) 1559–1565.
[12] V.C. Srivastava, M.M. Swamy, I.D. Mall, B. Prasad, I.M. Mishra, Coll. Surf. A 272 (2006) 89–104.
[13] X. Liu, G. Yu, W. Han, J. Hazard. Mater. 147 (2007) 746–751.
[14] W. Kim, T. Tachikawa, T. Majima, W. Choi, J. Phys. Chem. C 113 (2009) 10603–10609.
[15] J. Zhao, C. Chen, W. Ma, Top. Catal. 35 (2005) 269–278.
[16] A.A. Balandin, Nat. Mater. 10 (2011) 569–581.
[17] Y. Chen, L. Chen, L. Bai, L. Li, J. Mater. Chem. A 1 (2013) 1992–2001.
[18] S. Abdolhosseinzadeh, H. Asgharzadeh, S. Sadighikia, A. Khataee, Res. Chem. Intermed. 42 (2016) 4479–4496.
[19] C.S. Cheng, J. Deng, B. Lei, A. He, X. Zhang, L. Ma, S. Li, C. Zhao, J. Hazard. Mater. 263 (Pt 2) (2013) 467–478.
[20] M. Moshari, M. Rabbani, R. Rahimi, Res. Chem. Intermed. 42 (2016) 5441–5455.
[21] Z.Y. Sui, Y. Cui, J.H. Zhu, B.H. Han, ACS Appl. Mater. Interfaces 5 (2013) 9172–9179.
[22] Y. He, Y. Liu, T. Wu, J. Ma, X. Wang, Q. Gong, W. Kong, F. Xing, Y. Liu, J. Gao, J. Hazard. Mater. 260 (2013) 796–805.
[23] Y. Xu, Q. Wu, Y. Sun, H. Bai, G. Shi, ACS nano 4 (2010) 7358–7362.
[24] B. Qiu, M. Xing, J. Zhang, J. Am. Chem. Soc. 136 (2014) 5852–5855.
[25] B. Qiu, Y. Zhou, Y. Ma, X. Yang, W. Sheng, M. Xing, J. Zhang, Sci. Rep. 5 (2015) 8591.
[26] Y. Lei, F. Chen, Y. Luo, L. Zhang, Chem. Phys. Lett. 593 (2014) 122–127.
[27] B. Yu, J. Xu, J.-H. Liu, S.-T. Yang, J. Luo, Q. Zhou, J. Wan, R. Liao, H. Wang, Y. Liu, J. Environ. Chem. Eng. 1 (2013) 1044–1050.
[28] J.-S. Cheng, J. Du, W. Zhu, Carbohydr. Polym. 88 (2012) 61–67.
[29] J. Li, F. Wang, C.Y. Liu, J. Colloid Interface Sci. 382 (2012) 13–16.
[30] Y. Li, W. Cui, L. Liu, R. Zong, W. Yao, Y. Liang, Y. Zhu, Appl. Catal. B: Environ. 199 (2016) 412–423.
[31] Z. Zhang, F. Xiao, Y. Guo, S. Wang, Y. Liu, ACS Appl. Mater. Interfaces 5 (2013) 2227–2233.
[32] X. Yang, H. Cui, Y. Li, J. Qin, R. Zhang, H. Tang, ACS Catal. 3 (2013) 363–369.
[33] L. Liu, J. Liu, D.D. Sun, Catal. Sci. Technol. 2 (2012) 2525.
[34] M. Zhu, P. Chen, M. Liu, Langmuir: ACS J. Surf. Colloids 29 (2013) 9259–9268.
[35] M. Zhu, P. Chen, M. Liu, Acs Nano 5 (2011) 4529–4536.
[36] M. Ge, N. Zhu, Y. Zhao, J. Li, L. Liu, Ind. Eng. Chem. Res. 51 (2012) 5167–5173.
[37] W. Wang, J. Yu, Q. Xiang, B. Cheng, Appl. Catal. B: Environ. 119–120 (2012) 109–116.
[38] Y. Wang, R. Shi, J. Lin, Y. Zhu, Appl. Catal. B: Environ. 100 (2010) 179–183.
[39] X. Wang, S. Meng, X. Zhang, H. Wang, W. Zhong, Q. Du, Chem. Phys. Lett. 444 (2007) 292–296.
[40] Q. Liang, Y. Shi, W. Ma, Z. Li, X. Yang, Phys. Chem. Chem. Phys. 14 (2012) 15657.
[41] P. Dong, Y. Wang, B. Cao, S. Xin, L. Guo, J. Zhang, F. Li, Appl. Catal. B: Environ. 132–133 (2013) 45–53.
[42] I. Bautista-Toledo, M.A. Ferro-Garcia, J. Rivera-Utrilla, C. Moreno-Castilla, F. Vegas Fernández, J. Environ. Sci. Technol. 39 (2005) 6246–6250.
[43] Z.-M. Wang, H. Ooga, T. Hirotsu, W.-L. Wang, Q.Y. Wu, H.-Y. Hu, Appl. Clay Sci. 104 (2015) 81–87.
[44] L. Yang, Z. Li, H. Jiang, W. Jiang, R. Su, S. Luo, Y. Luo, Appl. Catal. B: Environ. 183 (2016) 75–85.